Ma et al. Breast Cancer Research (2025) 27:74
https://doi.org/10.1186/s13058-025-02039-0

Breast Cancer Research

RESEARCH Open Access

CPT1A/HIF-1α positive feedback loop induced fatty acid oxidation metabolic pathway contributes to the L-ascorbic acid-driven angiogenesis in breast cancer

Xiao Ma[1,2†], Baojian Zhang[1†], Xuezhe Yin[1], ShiPeng Yang[1], Zhenhua Lin[1,2], Yang Yang[1,2*] and Xianchun Zhou[1*]

Abstract

Background In tumors rich in adipose tissue, angiogenesis is a critical factor in promoting cancer cell metastasis. However, the connection between angiogenesis and the mechanisms driving adipose metabolic remodeling in breast cancer (BC) remains insufficiently understood. This research seeks to explore whether and how CPT1A, a crucial rate-limiting enzyme in fatty acid oxidation (FAO), supports angiogenesis through metabolic pathways in BC.

Methods First, cell functional assays and animal models were employed to elucidate the pro-carcinogenic effects of CPT1A on BC and its role in metabolic alterations. Following this, the reciprocal regulatory relationship between CPT1A and HIF-1α was elucidated using transcriptomic studies, ubiquitination analysis, and dual-luciferase assays. Matrigel tube formation assays, vasculogenic mimicry assays, and chick chorioallantoic membrane (CAM) assays were utilized to evaluate the effect of CPT1A on the pro-angiogenic properties of BC. Subsequently, untargeted metabolomics was employed to identify specific metabolic changes in supernatants with and without CPT1A expression and verified by functional recovery experiments. Finally, the prognostic significance of CPT1A and the vascular marker VEGF in BC tissues was evaluated using tissue microarrays and public databases.

Results CPT1A overexpression significantly enhanced cell proliferation, motility, and angiogenesis via activating the FAO metabolic pathway, as demonstrated by both in vivo and in vitro experiments. Mechanistically, CPT1A regulates the ubiquitination level of hypoxia-inducible factor-1α (HIF-1α), which directly binds to the CPT1A promoter. Mutations at the 63–74 and 434–445 regions significantly reduced CPT1A promoter activity, indicating that these sites are critical for its transcriptional regulation. Ultimately, this interaction creates a reinforcing feedback loop between CPT1A and HIF-1α. Subsequently, this feedback loop alters changes in extracellular L-ascorbic acid (LAA) levels. Interestingly, LAA affects ROS homeostasis through the Nrf2/NQO1 pathway, specifically influencing angiogenesis in BC and HUVECs, while having no significant effect on their proliferation or EMT process. Moreover, increased

†Xiao Ma and Baojian Zhang contributed equally to this work.

*Correspondence:
Yang Yang
yangyang@ybu.edu.cn
Xianchun Zhou
xczhou@ybu.edu.cn

Full list of author information is available at the end of the article

expression levels of CPT1A and vascular endothelial growth factor (VEGF) were significantly associated with lymph node metastasis and adverse outcomes in BC patients.

Conclusion The CPT1A/HIF-1α positive feedback loop critically regulates angiogenesis through activation of the Nrf2/NQO1 pathway, modulated by LAA. These findings highlight CPT1A and VEGF as promising therapeutic targets and prognostic biomarkers for angiogenesis in BC.

Research highlights

- CPT1A drives BC carcinogenesis through activation of the FAO metabolic pathway.
- CPT1A and HIF-1α form a reciprocal feedback loop that plays a central role in remodeling lipid metabolic pathways in BC.
- LAA uptake reduced by CPT1A/HIF-1α only promotes the angiogenesis via Nrf2/NQO1 pathway.
- High CPT1A/VEGF expression serves as an angiogenic factor and a reliable prognostic marker in BC.

Keywords Breast cancer, CPT1A/HIF-1α, Angiogenesis, Fatty acid oxidation, VEGF, L-ascorbic acid

Graphical abstract

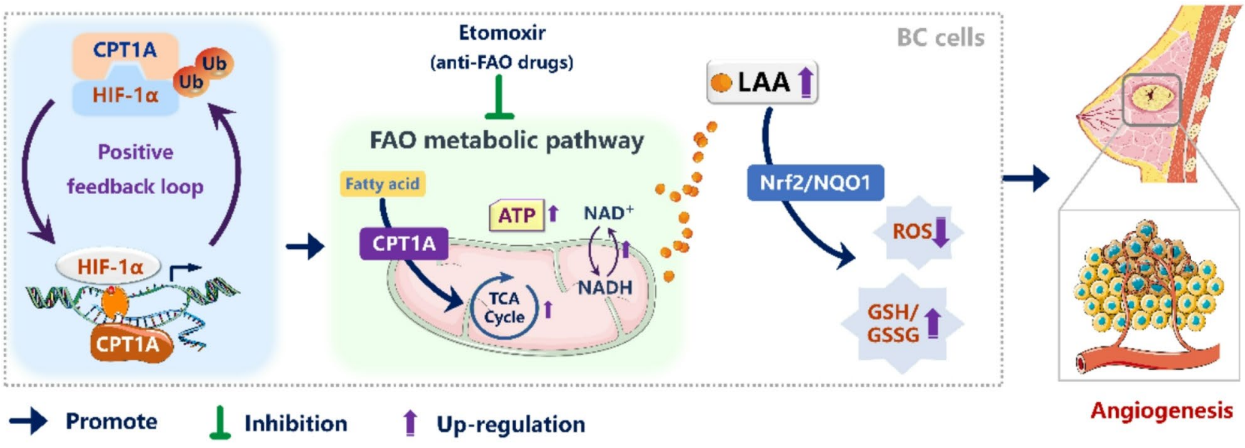

Introduction

Breast cancer (BC) is the most prevalent neoplasm in women, with metastasis serving as a critical driver of its aggressiveness and associated high mortality rates [1]. Angiogenesis has been identified as a key event that precedes the transformation of breast hyperplasia into malignancy, as it facilitates the enhanced blood supply necessary to meet the energy and nutrient demands of BC progression [2–4]. While drugs targeting tumor-associated blood vessels are extensively employed in cancer therapy, their therapeutic benefits in improving survival remain limited, primarily due to the development of anti-angiogenic drugs resistance [5]. This resistance is especially evident in cancers situated near adipose tissues, such as BC, pancreatic cancer, colon cancer, and hepatocellular carcinoma. These tumors frequently exhibit either inherent or acquired resistance to antiangiogenic therapy. For example, pancreatic ductal adenocarcinoma demonstrates intrinsic resistance, while colorectal cancer often develops evasive resistance to bevacizumab [6]. Consequently, a deeper understanding of the regulatory mechanisms connecting metabolism and angiogenesis is essential for developing innovative and more effective therapeutic strategies against BC.

Reprogramming cellular metabolism is critical to support the rapid growth and proliferation of tumors. Recent research has shown that highly proliferative cancer cells accomplish this by increasing lipogenic activity, which involves both the uptake of external lipids and the stimulation of internal lipid biosynthesis pathways [7]. In particular, this is especially true in non-glycolytic cancers such as prostate cancer and B-cell lymphoma where exogenous free fatty acids are utilised to generate energy via the fatty acid oxidation (FAO) pathway [8, 9]. Key enzymes in fatty acid metabolism, including Long-Chain Acyl-CoA Dehydrogenase (LCAD) and Medium-Chain Acyl-CoA Dehydrogenase (MCAD), are often overexpressed in invasive tumors, and their elevated levels are strongly associated with poor prognosis [10, 11]. CPT1 is the rate-limiting enzyme of FAO and CPT1A and CPT1C are commonly overexpressed in various human tumors [12]. Evidence suggests that CPT1A-mediated FAO promotes cancer cell proliferation, survival, and invasion [13]. For example, mitochondrial STAT3 has been shown to enhance FAO by stabilizing CPT1A through USP50

in macrophages [14]. Furthermore, CPT1A is implicated in BC-associated lymphangiogenesis via VEGF signaling [15]. Research has also shown that anti-VEGF therapies and tissue hypoxia enhance lipid transport and storage in cancer cells via an HIF-1α-dependent mechanism [16]. Importantly, HIF-1α expression enables tumor cells to evade therapeutic targets, thereby contributing to drug resistance [17]. Consequently, a comprehensive understanding of the regulatory mechanisms driving CPT1A-mediated metabolism and angiogenesis is crucial for devising innovative therapeutic approaches for BC.

Hypoxia can also affect the composition of different cell types within the tumor microenvironment, leading to alterations in cancer aggressiveness and responsiveness to therapy [18]. Interestingly, recent studies suggest that antioxidants may paradoxically promote angiogenesis and tumor progression through specific metabolic pathways [19, 20]. For example, antioxidants such as L-ascorbic acid (LAA) and glutathione can protect vascular endothelial cells by mitigating oxidative stress-induced damage [21, 22]. However, oxidative stress functions as a double-edged sword; its dysregulation can lead to DNA damage, mutations, and tumorigenesis. It is worth noting that vitamin C (commonly referred to as LAA) exhibits pro-oxidant properties when present at elevated concentrations [23]. In vivo studies have demonstrated that high doses of vitamin C can suppress the growth of intestinal tumors in Apc/KrasG12D mutant mice [24]. Moreover, clinical trials have shown that ascorbic acid in the blood and extracellular fluid significantly improves survival in patients with advanced cancer [25]. Its pro-oxidant effects on cancer cells are particularly enhanced by the inhibition of the transcription factor HIF-1α [26]. This process may involve altered extracellular uptake, which ultimately promotes BC angiogenesis and metastasis. However, the precise connection between CPT1A, HIF-1α, and LAA remains to be further elucidated.

In this study, we identified a novel positive feedback loop, CPT1A/HIF-1α, which acts as a central mechanism driving metabolic reprogramming in BC. This loop promotes BC progression by activating the FAO metabolic pathway. Additionally, reduced LAA uptake mediated by CPT1A/HIF-1α facilitates angiogenesis specifically through the Nrf2/NQO1 pathway and the regulation of ROS homeostasis. Notably, targeting the HIF-1α/CPT1A/VEGF axis effectively disrupts this pathological cycle, underscoring its potential as both a promising therapeutic target for anti-angiogenic therapy and a reliable prognostic marker in BC.

Materials and methods

Clinical samples

The tissue microarray consists of BC tissues and adjacent normal tissues, accompanied by patient survival data, comprehensive clinical information, and informed consent (Shanghai Outdo Biotech Co., Ltd.). Approval for the study was obtained from the Ethics Committee of Yanbian University, located in Yanji, China (approval number: YD20220406015). All patients were evaluated based on the World Health Organization's grading criteria for BC.

Cell culture and transfection

The MDA-MB-231, MCF-7, and HUVEC cell lines were sourced from ATCC and cultured in DMEM medium supplemented with 10% FBS, 0.1 mg/mL streptomycin, and 100 U/mL penicillin, maintained in a 5% CO_2 atmosphere at 37 °C. All cell lines were authenticated and characterized by the supplier before use. Stable transfections were performed using Lenti-shCPT1A-GFP, Lenti-CPT1A-GFP, Lenti-Vector, and Lenti-CPT1A obtained from Cyagen Biosciences (Guangzhou, China). Following transfection, clones were selected using puromycin at a concentration of 5 μg/mL. Cancer cells were co-transfected with control vectors or vectors containing HIF-1α fragments with lentiviral packaging mixtures (ATCC, USA) using Lipofectamine 3000 (Invitrogen, USA). The specific sequences are provided in Table S1.

Antibodies

Antibodies against Ki67 (No. 27309, 1:200), ZEB2 (14026-1-AP, 1:1000), Snail (13099-1-AP, 1:1000), E-cadherin (20874-1-AP, 1:20000), MMP9 (10375-2-AP, 1:1000), MMP2 (10373-2-AP, 1:20000), MCAD (55210-1-AP, 1:2000), LCAD (17526-1-AP, 1:2000), TWIST (25465-1-AP, 1:1000), Vimentin (110366-1-AP, 1:5000), CPT1A (15184-1-AP, 1:5000), HIF-1α (20960-1-AP, 1:3000), β-Tubulin (10068-1-AP, 1:1000), Nrf2 (16396-1-AP, 1:2000), and NQO1 (11451-1-AP, 1:2000) were purchased from Proteintech (Humanzyme), China. VEGF-A (YT4870, 1:1000) was purchased from Immunoway, California, USA.

Western blot

After washing the cells with PBS, RIPA lysis buffer (Solarbio, Beijing, China) supplemented with Protease Inhibitor Cocktail (Med Chem Express) was added, and the cells were lysed on ice for 30 min. The lysate was carefully collected using a spatula and transferred into a tube. Proteins were then extracted by centrifugation. The quantified proteomic samples were separated by SDS-PAGE based on protein size and subsequently transferred onto a polyvinylidene difluoride (PVDF) membrane (Millipore). The PVDF membrane was blocked with 5% skimmed milk, incubated overnight with the primary antibody, and subsequently incubated with the secondary antibody for 1 h at room temperature (RT). Protein bands were detected by Omni-ECL™ Ultrasensitive

Chemiluminescence Detection Kit (Epizyme, Shanghai, China) and visualised with a touch imager (e-BLOT).

5-ethynyl-2'-deoxyuridine (EdU) assay

The 5-ethynyl-2'-deoxyuridine (EdU) assay incorporates 5-ethynyl-2'-deoxyuridine into newly synthesized DNA within cells. The Cell-Light EdU Apollo 488 In Vitro Imaging Kit (C10310-3, RiboBio, China) was used according to the manufacturer's instructions and analyzed using an Olympus SZX10 microscope.

Matrigel tube formation assays

The pipette tips and centrifuge tubes required for the experiment were precooled at 4 °C. FBS-free DMEM medium and Matrigel gel were mixed at a 1:1 ratio, and 60μL of the Matrigel matrix gel diluent was added to each well of a 96-well plate, spread evenly to avoid bubbles, and solidified overnight for later use. Human Umbilical Vein Endothelial Cells (HUVECs) were digested, centrifuged, and resuspended in the culture medium. A total of 4×10^4 cells were mixed with 100μL of CPT1A differential expression cell-conditioned medium and 50μL of DMEM, spread on the Matrigel, and incubated in an incubator. Microtubule formation was observed under a microscope within 2–4 h, and images were captured.

Vasculogenic mimicry assays

Matrigel matrix gel was spread in a 96-well plate as described previously. BC cells were digested, centrifuged, resuspended in culture medium, and counted after preparation of the cell suspension. A total of 5×10^4 cells were added to each well, diluted with 150μL of medium, and evenly spread onto the Matrigel. The cells were incubated for 2–4 h, and tube formation was observed under a microscope. Images were then captured for analysis.

Immunohistochemistry (IHC)

Tissue microarrays and mouse tumor tissue sections were brought to room temperature and deparaffinized in an oven at 65 °C for 1 h. To block endogenous peroxidase activity, the tissue sections were treated with 3% H_2O_2 for 15 min. Following this, the sections were left to incubate overnight at 4 °C with the specified primary antibodies: Ki67 (No. 27309, 1:200), E-cadherin (20874-1-AP, 1:200), Vimentin (110366-1-AP, 1:200), CPT1A (15184-1-AP, 1:200), and VEGF-A (YT4870, 1:100). The secondary antibody was then incubated for one hour. Staining intensity was assessed under a microscope using diaminobenzidine (DAB) as the reagent, with hematoxylin (ZSGB-BIO) serving as the counterstain. Two pathologists evaluated the tissue specimens using a controlled, double-blind approach. A semi-quantitative technique was employed to assess both the extent of the positive staining area and the intensity of staining. Positive staining was characterized by the appearance of brownish-yellow granular deposits in the cytoplasm or nucleus. The staining intensity score was determined as follows: "- = 0," "+ = 1," "++ = 2," and "+++ = 3." The score was subsequently multiplied by the percentage of stained cells to calculate the staining index, with scoring as follows: ≤25% = 1, 26–50% = 2, 51–75% = 3, >75% = 4, which ranged from 0 to 12. Based on the staining index, scores were classified as negative (-) for 0–1, weak positive (+) for 2–4, moderate positive (++) for 5–7, and strong positive (+++) for 8 or higher. Tissue sections with scores of "++" or "+++" were categorized as strongly positive, indicating high expression of the corresponding antibody.

Immunoprecipitation (Co-IP) and detection of ubiquitination

BC cells were lysed using IP lysis buffer (Beyotime, China). Lysates were incubated with CPT1A and HIF-1α antibodies overnight at 4 °C, followed by the addition of protein A/G agarose beads (Med Chem Express) and incubation for 6 h. The beads were washed three times with cold lysis buffer for 5 min each time. An appropriate volume of eluent was added to an EP tube, combined with 2×SDS buffer, heated in a 95 °C metal bath for 5 min, and then analyzed via Western blotting. For the ubiquitination assay, cells were pretreated with MG132 (10 μM) for 8 h, collected using IP lysis buffer, and processed following the same procedure described above. Ubiquitination was analyzed by Western blot using an anti-Ubiquitin (Proteintech, China).

Dual-luciferase reporter assays

BC cells were seeded in 6-well plates at a density suitable for reaching 70–80% confluence for transfection with the HIF-1α overexpression plasmid. Following this, HIF-1α overexpressing BC cells were transferred to 96-well plates. Twenty-four hours post-seeding, these cells were transfected with *CPT1A*-luc reporter plasmids and a Renilla luciferase control plasmid using Lipofectamine 3000, according to the manufacturer's instructions. Forty-eight hours after transfection, cells were lysed using Passive Lysis Buffer, and luciferase activity was quantified with the Dual-Luciferase® Reporter Assay System (Promega, Cat#E1960).

Quantification of FAO, ATP, GSH/GSSG and NADPH

FAO levels in cell supernatants were quantified using the FAO ELISA kit (Shanghai Enzyme-linked Biotechnology Company, China). Intracellular GSH levels were measured using the GSH and GSSG Assay Kit (Beyotime, China), while intracellular ATP and NADPH levels were determined using the ATP and NADPH assay kits (Nanjing Jiancheng Bioengineering Institute, China). All

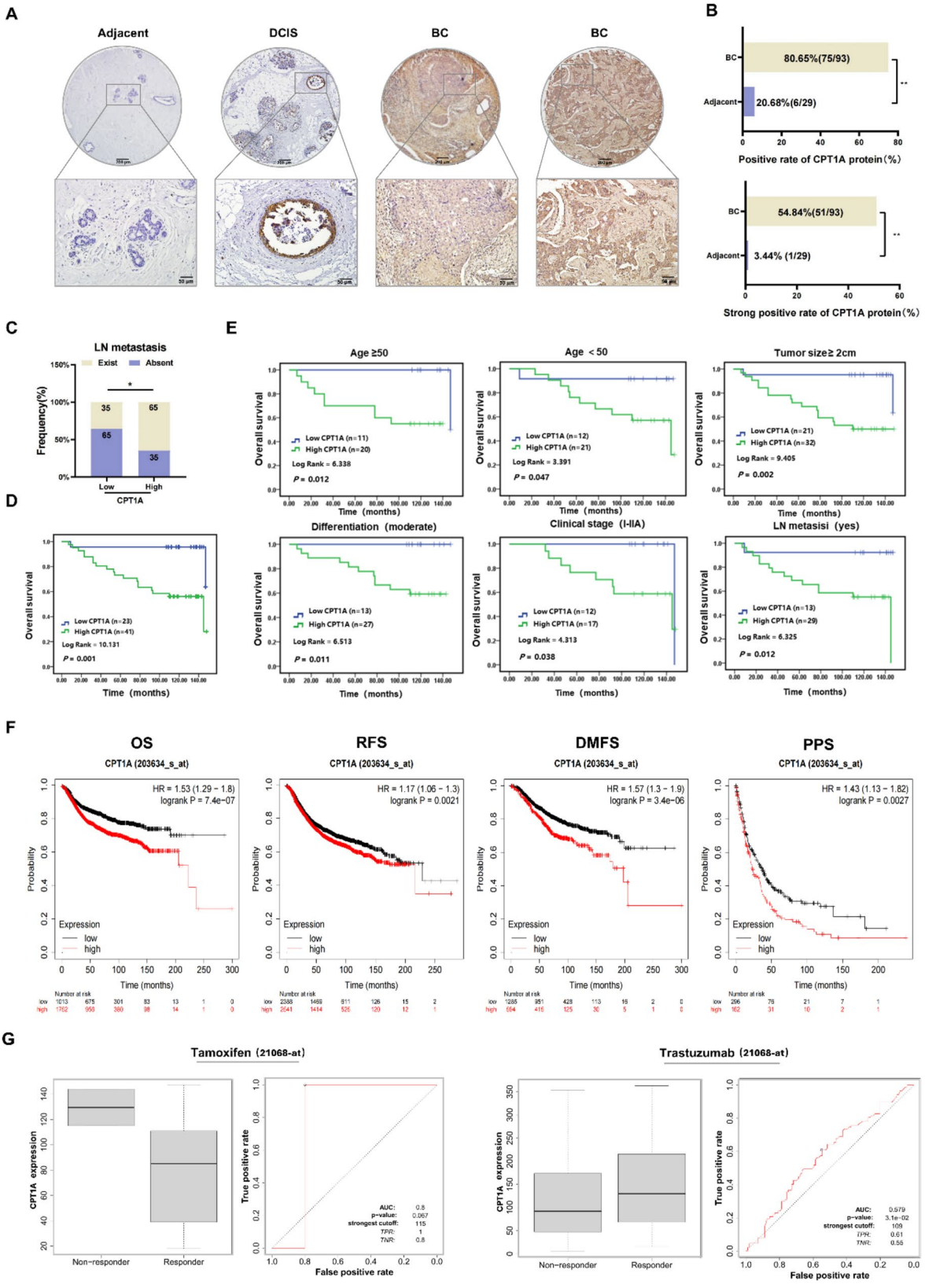

Fig. 1 (See legend on next page.)

(See figure on previous page.)

Fig. 1 The upregulation of CPT1A is associated with increased malignancy and a worse prognosis in BC. (**A**) Representative IHC staining images of CPT1A. Scale bar: 200 μm (Up) and 50 μm (Down). (**B**) The positive and strong positive rate of CPT1A protein expression in adjacent normal ($n = 29$) and BC ($n = 93$) tissues. (**C**) Distribution of existing and absent LN metastasis in the CPT1A-low and CPT1A-high groups. (**D**) Kaplan-Meier survival analysis of BC in patients ($n = 64$) with low or high CPT1A expression ($P = 0.001$). (**E**) Correlation between CPT1A expression and the clinicopathological significance of patients with BC. (**F**) Overall survival (OS), recurrence-free survival (RFS), distant metastasis-free survival (DMFS), and post-progression survival (PPS) analysis of BC patients with CPT1A low or high expression in Kaplan-Meier databases. (**G**) Chemotherapy response rate and ROC analysis of CPT1A and BC patients in the Kaplan-Meier database. $^{*}P < 0.05$, $^{**}P < 0.01$

measurements were performed according to the manufacturers' instructions.

LC-MS analysis of metabolites

MDA-MB-231-shNC or MDA-MB-231-shCPT1A cells were grown in Petri dishes to a suitable density. The collected supernatants were spun at 13,300 rpm for 4 min and subsequently stored at -80 °C prior to analysis. Metabolomic analyses were conducted at the Shanghai Applied Protein Technology Co., Ltd.

Chick Chorioallantois Membrane (CAM) assay

Specific pathogen-free fertilized chicken eggs were chosen and incubated in an automatic incubator for about 8 days. A small window was created in the eggshell, and the eggshell membrane was separated to expose the CAM. A sterile ring was placed over the blood vessels to observe angiogenesis. Next, 2×10^6 cells were added to the exposed CAM, the egg was sealed with sterile tape, and incubation continued for 48 h. The CAM was photographed using a microscope (Olympus SZX10).

In vivo assays for tumorigenesis and metastasis

All animal experiments and procedures were approved by the Animal Research Ethics Committee of Yanbian University. Female BALB/c nude mice aged 4–5 weeks were bred under specific pathogen free conditions. MDA-MB-231 cells, with differential expression of CPT1A, as well as control cells, were routinely digested, centrifuged, resuspended, and counted (3×10^5 cells/mice). The nude mice were randomly divided into two groups, with five mice in each group. In group A, sh-Con cells were injected into the left axilla, and sh-CPT1A cells were injected into the right axilla. In group B, Vector cells were injected into the left axilla, and cells overexpressing CPT1A were injected into the right axilla [28]. The tumor volume and weighed was measured every 2 days using calipers and calculated using the standard formula (length × width^2 × 0.5). After 8 weeks, Mice were anesthetized with 2% isoflurane to minimize distress and subsequently euthanized. Fluorescence intensity was measured using the UVP iBOX® Scientia™ 900 imaging system (CA, USA). Tumors were then excised, weighed, and prepared for further analysis. In addition, to create a tumor metastasis model, MDA-MB-231 cells (1×10^6) were injected into the tail vein of nude mice. Eight weeks later, the mice were euthanized, and their lung tissues were harvested for immunohistochemical analysis.

Statistical analysis

Statistical analyses were carried out using SPSS 25 software (IBM Corp.), GraphPad Prism 9.0, and ImageJ. Data were gathered from three independent experiments and are presented as mean ± SEM. To evaluate statistical differences between two groups, an unpaired t-test was used, while one-way ANOVA facilitated comparisons among multiple groups. The χ^2 test assessed the correlation between CPT1A protein expression and clinicopathological parameters. Survival curves were plotted using the Kaplan-Meier method, with *P*-values obtained through the log-rank test. The relationship between CPT1A and VEGF expression levels was analyzed using Pearson's correlation test. Furthermore, Cox proportional hazards models were utilized to calculate hazard ratios in both univariate and multivariate logistic regression analyses.

Results

The upregulation of CPT1A is associated with increased malignancy and a worse prognosis in BC

Genetic alterations in CPT1A can result in aberrant expression in cancer. Analysis of the cBioPortal database confirmed that CPT1A amplification is highly significant in BC (Fig. S1A). CPT1A was significantly overexpressed in BC tissues (positive rate: 80.64%, strong positive rate: 54.84%, $P < 0.01$) compared to adjacent normal tissues (positive rate: 20.68%, strong positive rate: 3.44%, $P < 0.01$) (Fig. 1A, B, and Table 1). Furthermore, elevated expression of CPT1A was positively correlated with lymph node (LN) metastasis ($P < 0.005$), though it showed no association with age, tumor size, or degree of differentiation (Fig. 1C; Table 2). Cox univariate analysis revealed that CPT1A expression level ($P = 0.039$) and differentiation grade ($P = 0.003$) were independent prognostic indicators for patients with BC (Table 3). Patients with low CPT1A protein expression exhibited significantly longer overall survival (OS) rates than those with high CPT1A expression ($P = 0.001$) (Fig. 1D). Compared to patients aged ≤ 50 years ($P = 0.012$) and > 50 years ($P = 0.047$), those with tumor diameters ≥ 2 cm

Table 1 CPT1A protein expression in BC

Diagnosis	No. of cases	CPT1A protein expression				Positive rate	Strongly positive rate
		-	+	++	+++		
BC	93	18	24	25	26	80.64%	54.83%
Adjacent tissues	29	23	5	1	0	20.68%	3.44%

Positive rate: percentage of positive cases with +~+++ staining score

Strongly positive rate: percentage of positive cases with ++and +++ staining score

BC: Breast cancer

Table 2 Correlation between CPT1A expression and the clinicopathological features of BC

Variables	No. of cases	CPT1A strongly positive cases (%)	χ^2	*P* value
Age (years)	53	27 (50.94%)	0.755	0.385
>50	40	24 (60.00%)		
≤ 50				
Tumor size (cm)	75	40 (53.33%)	0.355	0.552
>2.0	18	11 (61.11%)		
≤ 2.0				
Grade	18	11 (61.11%)	1.562	0.458
I	58	33 (56.89%)		
II	17	7 (41.17%)		
III				
Clinical Stage	36	18 (50.00%)	0.555	0.456
I-IIA	57	33 (57.89%)		
IIB-IV				
LN metastasis	48	33 (68.75%)	7.752	**0.005***
Yes	45	18 (40.00%)		
No				
ER	32	22 (68.75%)	0.386	0.535
Positive	32	19 (59.37%)		
Negative				
PR	29	20 (68.96%)	0.554	0.457
Positive	35	21 (60.00%)		
Negative				
Her2	24	13 (54.16%)	1.633	0.201
Positive	40	28 (70.00%)		
Negative				
Ki-67	20	12 (60.00%)	0.209	0.648
Positive	44	29 (65.90%)		
Negative				
p53	28	19 (67.85%)	0.034	0.853
Positive	36	22 (61.11%)		
Negative				

* $P < 0.05$ and ** $P < 0.01$

($P = 0.002$), intermediate differentiation ($P = 0.011$), Stage I-IIA BC ($P = 0.038$), or LN metastasis ($P = 0.012$) demonstrated significantly reduced OS times (Fig. 1E). Interestingly, BC patients with high CPT1A expression showed shorter OS, recurrence-free survival (RFS), distant metastasis-free survival (DMFS), and post-progression survival (PPS) ($P < 0.01$) (Fig. 1F). Moreover, BC patients with high CPT1A expression exhibited a higher response rate to trastuzumab treatment but showed no response to tamoxifen therapy (Fig. 1G). These results indicate that CPT1A may be a potential novel molecular marker for targeted therapy in BC patients.

CPT1A enhances BC proliferation both in vivo and in vitro

To explore the molecular role of CPT1A in BC cells, we examined the expression of CPT1A in different BC cell lines, and MDA-MB-231 and MCF-7 cells were comprehensively selected as subsequent experiments (Fig.S2A). Then we generated stable cell lines with varying CPT1A expression levels, categorized into the following groups: Control (Con), sh-CPT1A, Vector, and CPT1A (Fig. 2A and S2B-E). The CPT1A overexpression group exhibited significantly higher cell viability and colony formation compared to the sh-CPT1A group (Fig. 2B, C). The incorporation rate of newly synthesized DNA labeled by the EdU probe (red) was also higher in the CPT1A overexpression group than in the sh-CPT1A group (Fig. 2D). Further experiments demonstrated that the G2/M% + S% proliferation rate in CPT1A-overexpressing cells exceeded that of CPT1A knockdown cells (Fig. 2E). Consistently, CPT1A overexpression increased subcutaneous tumor volume, tumor weight, and total fluorescence intensity, indicating a positive effect on tumor formation (Fig. 2F and S3A-C). And the CPT1A overexpression group showed an upregulation in Ki67 protein positivity, reflecting a high degree of tumor proliferation and malignancy (Fig. 2G and S3D). Furthermore, CPT1A overexpression was positively correlated with microvessel density, as indicated by CD31 staining in tumor tissues, suggesting a rich blood supply and enhanced invasive ability (Fig. S3E). These findings suggest that CPT1A plays a critical oncogenic role in BC development.

CPT1A partially accelerates BC metastasis through the EMT process

Tumor progression is marked by enhanced cell motility and invasiveness. The rate of scratch healing and vertical migration in BC cells was significantly inhibited by knockdown of CPT1A compared to control (Fig. 3A, B, and S4A, B). Extensive metastatic nodules were observed in the lungs of mice in the CPT1A overexpression group, accompanied by clear destruction of lung tissue structure and well-defined cancer nests (Fig. 3C, D). Interestingly, in the CPT1A knockdown group, BC cells exhibited a reduction in size and a rounded shape, while in the

Table 3 Univariate and multivariate survival analyses (Cox regression model) of various factors in 64 BC patients

Characteristics	B	SE	Wald	95% CI		*P*-value
				Lower	Upper	
Univariate survival analyses						
CPT1A	0.551	0.267	4.257	1.028	2.926	**0.039***
Age	-0.140	0.255	0.301	0.528	1.433	0.583
Tumor size	0.200	0.335	0.358	0.634	2.356	0.550
Differentiation	0.617	0.206	8.966	1.238	2.777	**0.003***
Clinical stage	0.146	0.254	0.330	0.703	1.903	0.566
LN metastasis	0.006	0.269	0.001	0.594	1.707	0.981
Multivariate survival analyses	0.740	0.226	10.720	1.346	3.263	**0.001****
Differentiation	-0.164	0.279	0.347	0.491	1.465	0.556
LN metastasis	0.66	0.276	5.877	1.137	3.355	**0.015***
CPT1A						

B: Coefficient; SE: standard error; Wald: Wald statistic; CI: confidence interval

* $P<0.05$ and ** $P<0.01$

CPT1A overexpression group, BC cells displayed prominent nuclear, an elongated spindle shape, and an increase in filopodia, indicating enhanced mesenchymal morphology (Fig. 3E and S4C). Additionally, the epithelial marker E-cadherin was upregulated, while mesenchymal markers (ZEB2, Vimentin, Snail, and Twist) were downregulated in the sh-CPT1A group, with the opposite observed in the CPT1A overexpression group (Fig. 3F and S4D). Immunofluorescence and IHC further confirmed that CPT1A overexpression decreased E-cadherin protein expression levels while increasing Vimentin expression (Fig. 3G, H). These findings suggest a strong correlation between CPT1A expression and the promotion of EMT in BC.

CPT1A promotes microtubule formation and angiogenesis in BC and HUVECs

Tumors are characterized by sustained angiogenesis, a key factor in tumor metastasis. Using the Matrigel tube formation assay, we observed that HUVECs exhibited enhanced angiogenic capacity when exposed to the supernatant from CPT1A-overexpressing BC cells (Fig. 4A and S4E). Furthermore, CPT1A-overexpressing BC cells formed vascular-like channels by remodeling and deforming the extracellular matrix, a process independent of endothelial cells (Fig. 4B and S4F). In vivo experiments revealed that angiogenesis was inhibited in the sh-CPT1A group, resulting in fragmented and dissolved vessels, whereas vessels in the CPT1A-overexpressing group remained intact and functional (Fig. 4C). Mechanistically, knocking down CPT1A markedly reduced the expression of critical angiogenic markers such as MMP2, MMP9, and VEGF. Conversely, overexpressing CPT1A resulted in the increased expression of these markers (Fig. 4D and S4G). To further explore this, HUVECs were cultured with BC cell supernatants with different CPT1A expression levels. The supernatant from CPT1A-overexpressing cells exhibited higher levels of angiogenic factors compared to control cells, promoting the wound healing ability, vertical migration, and proliferation of HUVECs. In contrast, the sh-CPT1A group exhibited reduced secretion of angiogenic factors, resulting in impaired angiogenic functions (Fig. 4E-G and S4H, I). These findings demonstrate that CPT1A enhances the angiogenic capacity of BC, contributing to tumor progression and metastasis.

CPT1A-driven FAO pathway promotes BC progression

Yan et al. reported that the CPT1A-driven FAO pathway promotes embryonic stem cell survival [27]. In our study, we demonstrated that the levels of FAO, ATP, and NADPH metabolism were significantly upregulated in the CPT1A-overexpression group (Fig. 5A). We then measured the oxygen consumption rate (OCR) and found that OXPHOS was reduced in CPT1A knockdown cells, indicating impaired mitochondrial respiration (Fig. S5A). Furthermore, CPT1A overexpression increased the levels of FAO markers, such as LCAD and MCAD, while these markers were downregulated in the knockdown group (Fig. 5B and S5B). A subsequent loss-of-function experiment verified that etomoxir (ETX, 15 μM) successfully suppressed the development of colonies and the lateral migration of BC cells driven by CPT1A overexpression (Fig. 5C, D, and S5C). Beyond its effects on BC cells, ETX also suppressed angiogenesis in HUVECs, causing the dissolution, bleeding, and coagulation of CAM blood vessels (Fig. 5E, F). Additionally, ETX blocked the CPT1A-driven FAO pathway, leading to reduced ATP and NADPH production (Fig. 5G). Consistently, ETX decreased FAO levels as well as markers of EMT progression and angiogenesis that were elevated by CPT1A overexpression (Fig. 5H and S5D). In conclusion, these findings suggest that the CPT1A-driven

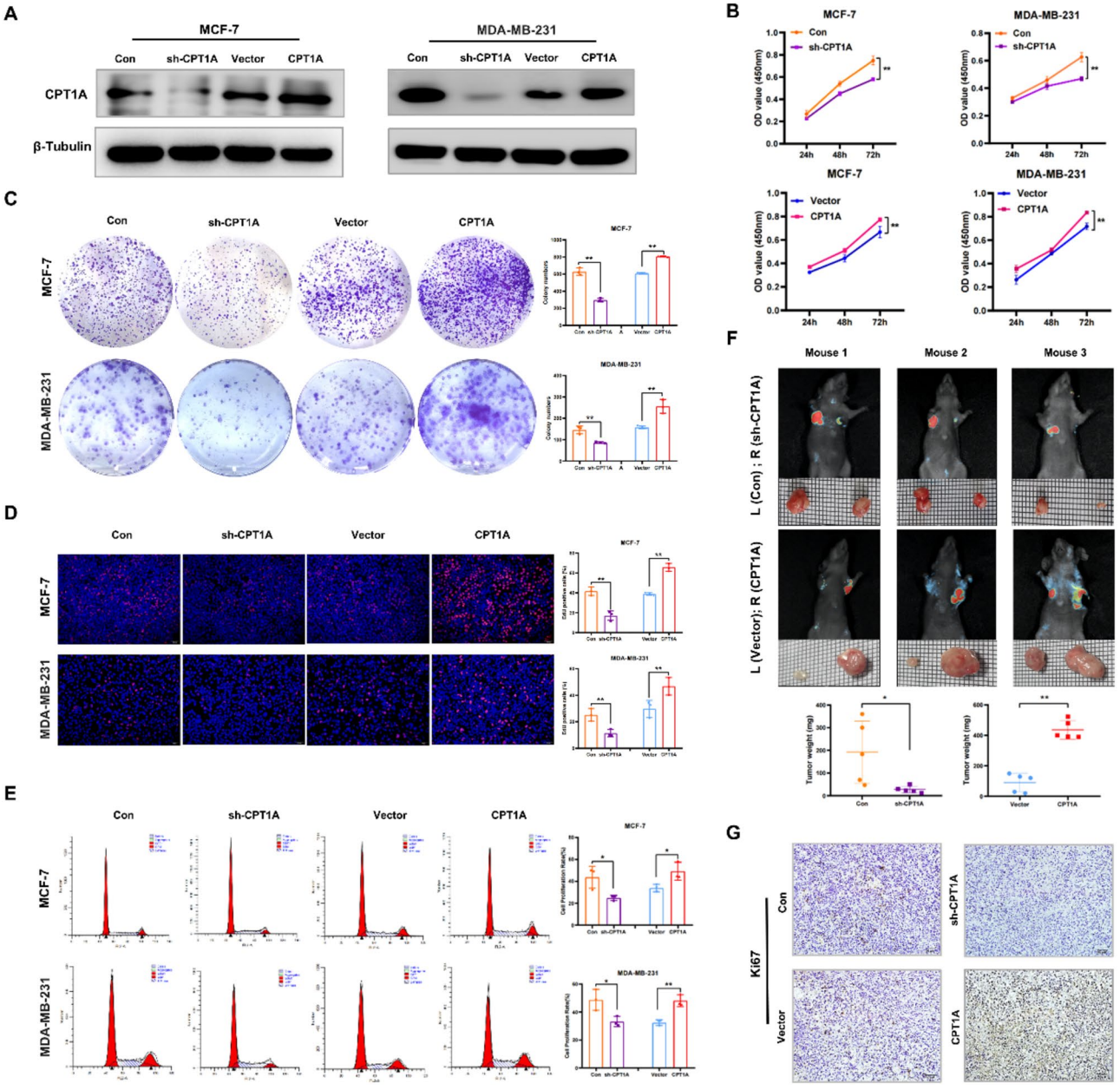

Fig. 2 CPT1A enhances BC proliferation both in vivo and in vitro. (**A**) CPT1A knockdown and overexpression BC cell lines were constructed, and the transfection efficiency was verified by Western blot. (**B-D**) BC cells proliferation ability was tested by CCK8 (**B**), colony formation (**C**) and EdU assays (**D**). Scale bar: 50 μm. (**E**) The ratio of G2/M%+S% in different groups was quantified by flow cytometry. Quantification of the flow cytometry result ($n = 3$). (**F**) Representative fluorescence imaging and morphology of the nude mice xenograft. The down panel represents the analysis of tumor volume and weight. Size of each grid: 1 mm × 1 mm. ($n = 5$). (**G**) IHC staining showed Ki67 expression in tumor specimens from xenografts. Scale bar: 50 μm. $^{*}P < 0.05$ and $^{**}P < 0.01$

FAO pathway plays a critical role in promoting EMT progression and angiogenesis in BC.

The CPT1A/HIF-1α positive feedback loop promotes the proliferation and metastasis of BC

KEGG metabolic pathway analysis revealed significant enrichment in the HIF-1α signaling pathway, indicating downregulation of HIF-1α in the sh-CPT1A group (Fig. 6A). And we found that the expression of CPT1A and HIF-1α in BC was positively correlated by database analysis, and RNAseq analysis of TCGA found that BC patients with high expression of CPT1A and HIF-1α had a worse prognosis (Fig. S6A-D). Furthermore, CPT1A and HIF-1α were shown to bind endogenously in BC cells (Fig. 6B). Significantly, MG132 treatment caused an increase in HIF-1α protein levels, with the effect being more prominent in the sh-CPT1A group. Additionally, HIF-1α degradation was induced by CHX, but

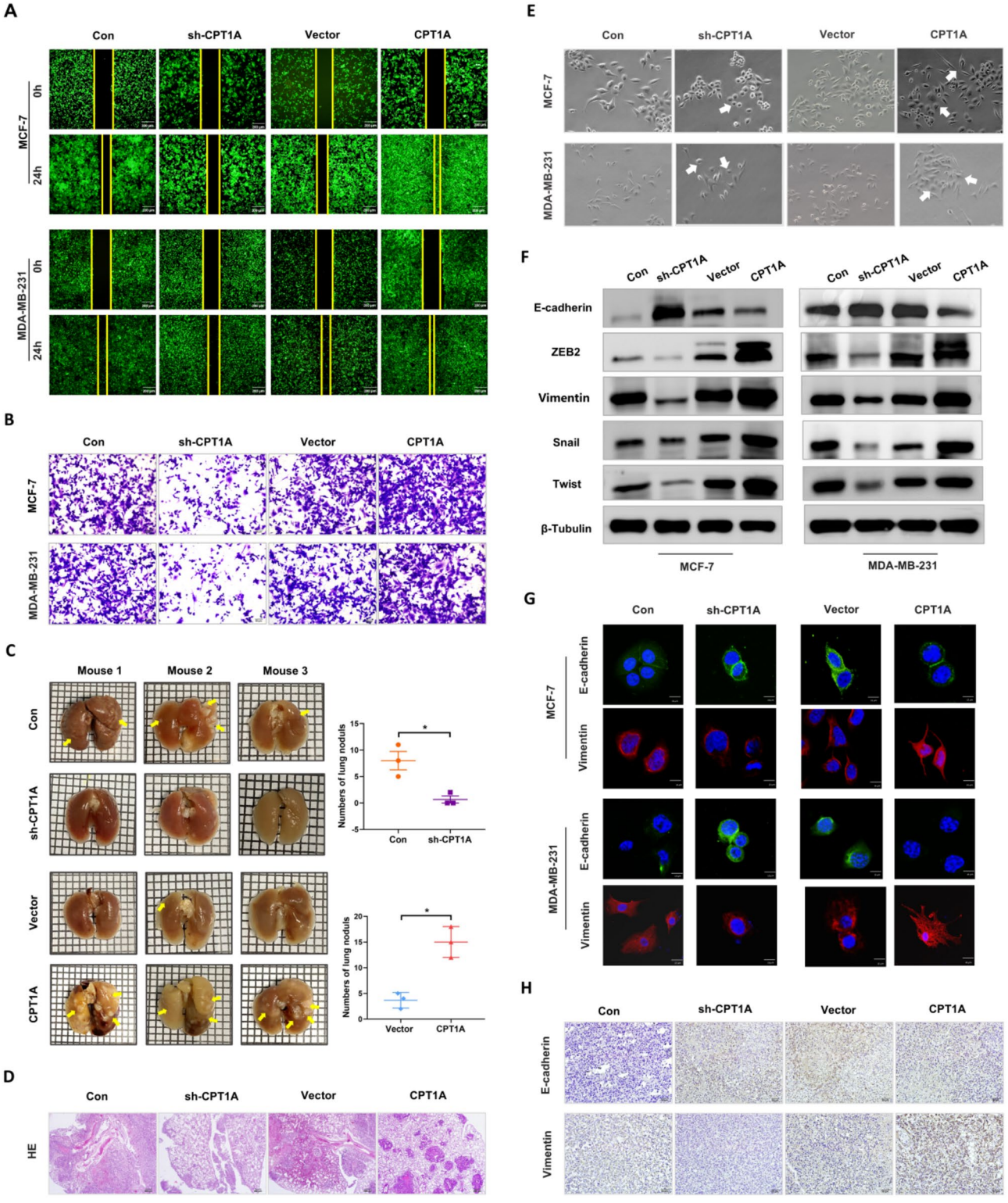

Fig. 3 (See legend on next page.)

this degradation was inhibited by CPT1A, indicating that CPT1A regulates the stability of HIF-1α (Fig. 6C). Ubiquitylation of HIF-1α was significantly elevated in sh-CPT1A cells compared to the control group (Fig. 6D). Reporter gene assays demonstrated that HIF-1α significantly increased the luciferase activity of a construct containing the CPT1A binding site, whereas this effect was attenuated in a mutant construct lacking the binding

(See figure on previous page.)

Fig. 3 CPT1A partially accelerates BC metastasis through the EMT process. (**A**) Representative images of CPT1A differentially expressed BC cells for scratch healing at 0 and 24 h after scratch. Wound healing percentage was quantified width of 24 h/0 h by Image J. Scale bar: 200 μm. (**B**) Representative images of the transwell (migration) assay of BC cells with differential CPT1A expression. Scale bar: 50 μm. (**C-D**) MDA-MB-231 cells with differential CPT1A expression cells were injected into the nude mice respectively via tail vein for in vivo metastasis ($n=3$). Representative images showed the number of lung metastasis nodules (**C**), and HE staining (**D**) of the lung tissues. Size of each grid: 1 mm × 1 mm. Scale bar: 200 μm. (**E**) Morphological changes of the four groups of BC cells. (**F**) Protein expression of EMT markers (E-cadherin, ZEB2, Vimentin, Snail, Twist) were detected by Western blot in CPT1A differentially expressed BC cells. (**G**) IF staining of E-cadherin and Vimentin in BC cells with differential expression of CPT1A (blue: nuclear staining; green: E-cadherin staining; red: Vimentin staining), Scale bar: 25 μm. (**H**) IHC staining of E-cadherin and Vimentin in the four groups of xenograft tumor tissues. Scale bar: 50 μm. *$P<0.05$ and **$P<0.01$

site (Fig. 6E). In rescue experiments, overexpression of HIF-1α in the sh-CPT1A group reversed the observed reductions in proliferation, lateral migration, and longitudinal migration (Fig. 6F-H and S6E-G). Shenoy et al. previously reported that HIF-1-dependent VEGF expression mediates angiogenesis and metastasis in BC cells. Consistent with this, the tube formation ability of HUVECs was restored by HIF-1α overexpression in the CPT1A knockdown group (Fig. S6H). Furthermore, HIF-1α overexpression reversed the reduction in FAO metabolism observed in sh-CPT1A cells (Fig. 6I). It also enhanced EMT progression and increased the expression of angiogenesis markers (Fig. 6J and S6I). Collectively, these findings demonstrate that the CPT1A/HIF-1α positive feedback loop plays a pivotal role in promoting BC proliferation, EMT progression, angiogenesis, and metastasis.

LAA uptake reduced by CPT1A/HIF-1α only promotes the angiogenesis via NRF2/NQO1 pathway

Key factors inducing angiogenesis in HUVECs from CPT1A supernatants were identified using LC-MS/MS. Among these, LAA, glutamine, and tyrosine levels were significantly altered in the sh-CPT1A group, with LAA showing the most pronounced difference (Fig. 7A). Notably, LAA did not affect BC cell proliferation, colony formation, or EMT progression (Fig. 7B, C, I, and S7A). However, the addition of LAA (5 μM) to sh-CPT1A supernatants enhanced tube formation in both HUVECs and BC cells (Fig. 7D, E, and S7B). Moreover, LAA treatment restored the ruptured and bleeding chorionic vessels observed in the sh-CPT1A group (Fig. 7F), although it did not influence the proliferation capacity of HUVECs (Fig. S7C, D). Consistently, LAA reversed the reduction in the wound-healing rate and increased the number of migrating HUVECs in the sh-CPT1A group (Fig. 7G, H, and S7E, F). Additionally, protein levels of angiogenesis markers were elevated in the sh-CPT1A group following LAA treatment (Fig. 7I and S7G).

To investigate how LAA promotes angiogenesis, we examined changes in extracellular homeostasis. The addition of LAA to the sh-CPT1A group significantly upregulated GSH/GSSG expression levels and reduced ROS production (Fig. 7J, K). Furthermore, we assessed ROS changes following LAA treatment using flow cytometry with DCFH-DA, and obtained consistent results (Fig. S7H). Additionally, LAA treatment enhanced the expression of key oxidative stress regulators, including Nrf2, NQO1, and HIF-1α (Fig. 7L and S7I). In conclusion, CPT1A facilitates angiogenesis in BC by regulating extracellular LAA uptake and oxidative stress levels, independent of EMT progression. These findings highlight endothelial cell metabolism as a promising therapeutic target for BC treatment.

High levels of CPT1A/VEGF expression are correlated with poor prognosis of patients with BC

Xiong et al. reported that CPT1A regulates BC-associated lymphangiogenesis via VEGF signaling [29]. Consistent with this, our findings revealed a significant positive correlation between CPT1A and VEGF expression in angiogenesis, which was stronger than the correlations observed with MMP2 and MMP9 (Fig. 8A). To further explore this relationship, we analyzed VEGF and CPT1A expression in normal tissues, DCIS, and BC tissues. Interestingly, CPT1A and VEGF protein expression levels were lower in normal tissues and higher in cancerous tissues (Fig. 8B), with a significant positive correlation identified in BC tissues ($P<0.05$) (Fig. 8C). Statistical analysis revealed that 54.84% of BC tissues with high CPT1A expression exhibited strong VEGF staining, whereas 45.16% of tissues with low CPT1A expression showed weak VEGF staining (Fig. 8D). These results were further validated by IHC score analysis, which aligned with findings from the UALCAN database (Fig. 8E, F). Additionally, chi-square analysis demonstrated a significant association between high VEGF expression and lymph node metastasis ($P<0.05$), supported by data from the UALCAN database (Fig. 8H). Furthermore, BC patients with high VEGF expression were found to have shorter overall survival times, indicating a poorer prognosis (Fig. 8I). In conclusion, these results indicate that the CPT1A/VEGF axis is essential for BC progression and may act as a valuable biomarker for predicting BC outcomes.

Discussion

During the process of angiogenesis, tumor cells heavily rely on aberrant metabolism and the state of their extracellular environment [30]. However, the regulatory role of CPT1A, a key enzyme in FAO metabolism, in

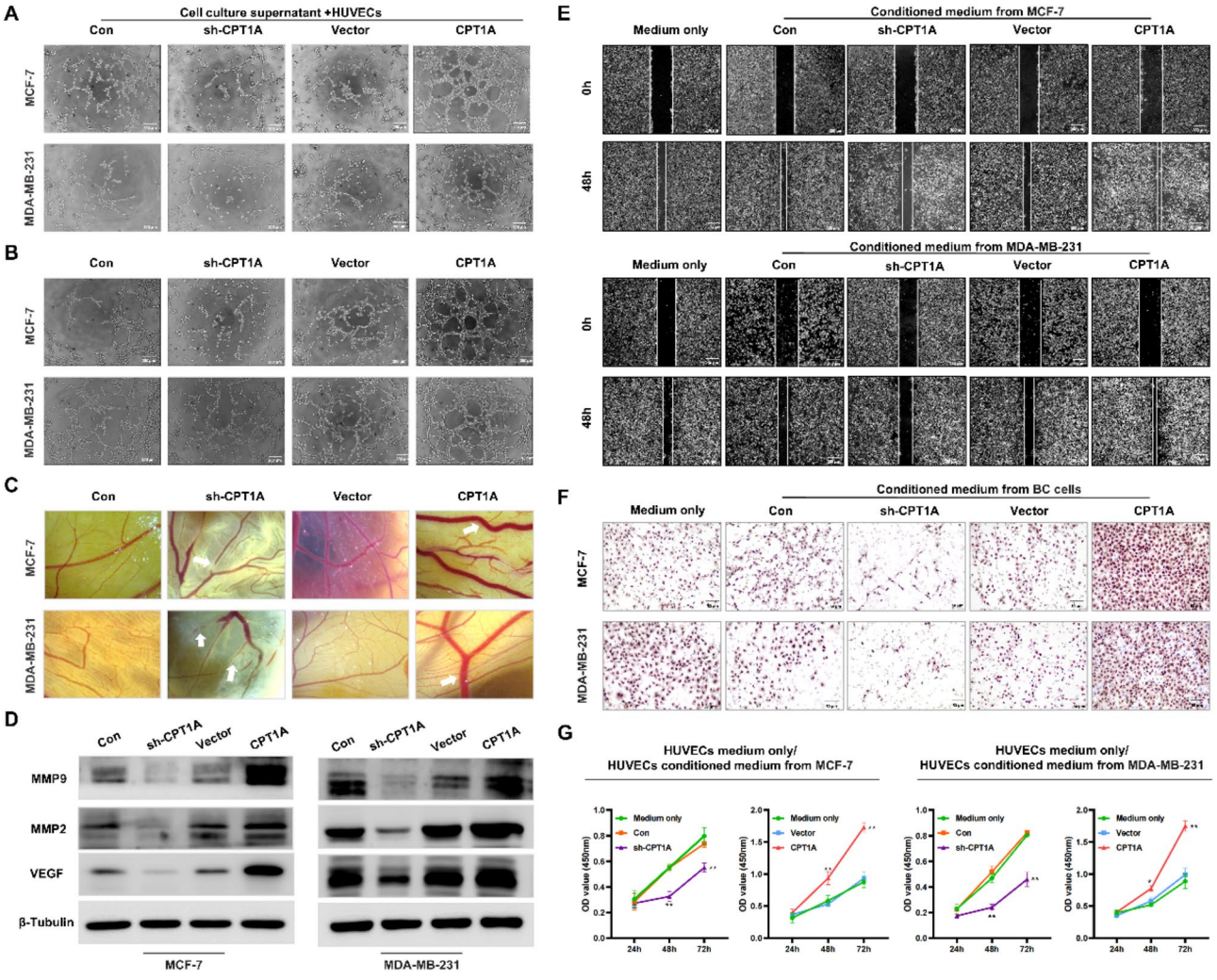

Fig. 4 CPT1A promotes microtubule formation and angiogenesis in BC and HUVECs. (**A**) HUVECs were cultured with the supernatants of BC cells, and the microtubule formations were detected by matrigel tube formation assay. (**B**) The vascular mimicry ability of the BC cells was detected by the vasculogenic mimicry assay. (**C**) The effect of CPT1A on ex vivo angiogenesis was assessed by CAM assay. The white arrows indicate the morphological changes in CAM. (**D**) Protein expression of angiogenesis markers (MMP2, MMP9, VEGF) was detected by Western blot in CPT1A differentially expressed BC cells. (**E-G**) HUVECs were cultured with medium and the supernatants of BC cells respectively. The migration ability of HUVEC cells was assessed by wound healing (**E**) and transwell assays (**F**), and the proliferation ability of HUVECs was detected by CCK8 assay (**G**). $^{*}P < 0.05$, $^{**}P < 0.01$

BC angiogenesis remains unclear. Our research demonstrates a reciprocal positive interaction between CPT1A and HIF-1α, which activates the FAO metabolic pathway and regulates LAA uptake, thereby inducing a pro-angiogenic cellular system in BC. CPT1A also enhanced VEGF expression levels, a key growth factor involved in angiogenesis [31]. These findings underscore the critical role of CPT1A/HIF-1α-mediated metabolic reprogramming in driving BC angiogenesis and nutrient absorption as the disease progresses.

Metabolic alterations have been observed to suppress the production of angiogenic and pro-inflammatory factors by BC cells, thereby reducing angiogenesis and impeding BC progression [32, 33]. Ma et al. demonstrated that targeting CPT1A can synergize with CD8 + T cells to promote tumor ferroptosis, leading to significant tumor regression [34]. In contrast, our findings showed that CPT1A-mediated FAO plays a critical role in BC metabolism, with CPT1A upregulation enhancing angiogenesis and growth potential. This adaptation likely enables BC cells to survive in harsh environments, such as energy deprivation, by reorganizing their metabolic processes to withstand extracellular stresses [35]. Consistent with this, Cao et al. reported that CPT1A upregulation significantly increases the production of intermediates in the nucleoside metabolism pathway and promotes the cell cycle in nasopharyngeal carcinoma [36]. Similarly, Wang et al. and Shao et al. found that CPT1A-mediated fatty acid oxidation increases metastatic capacity and anoikis resistance in colorectal

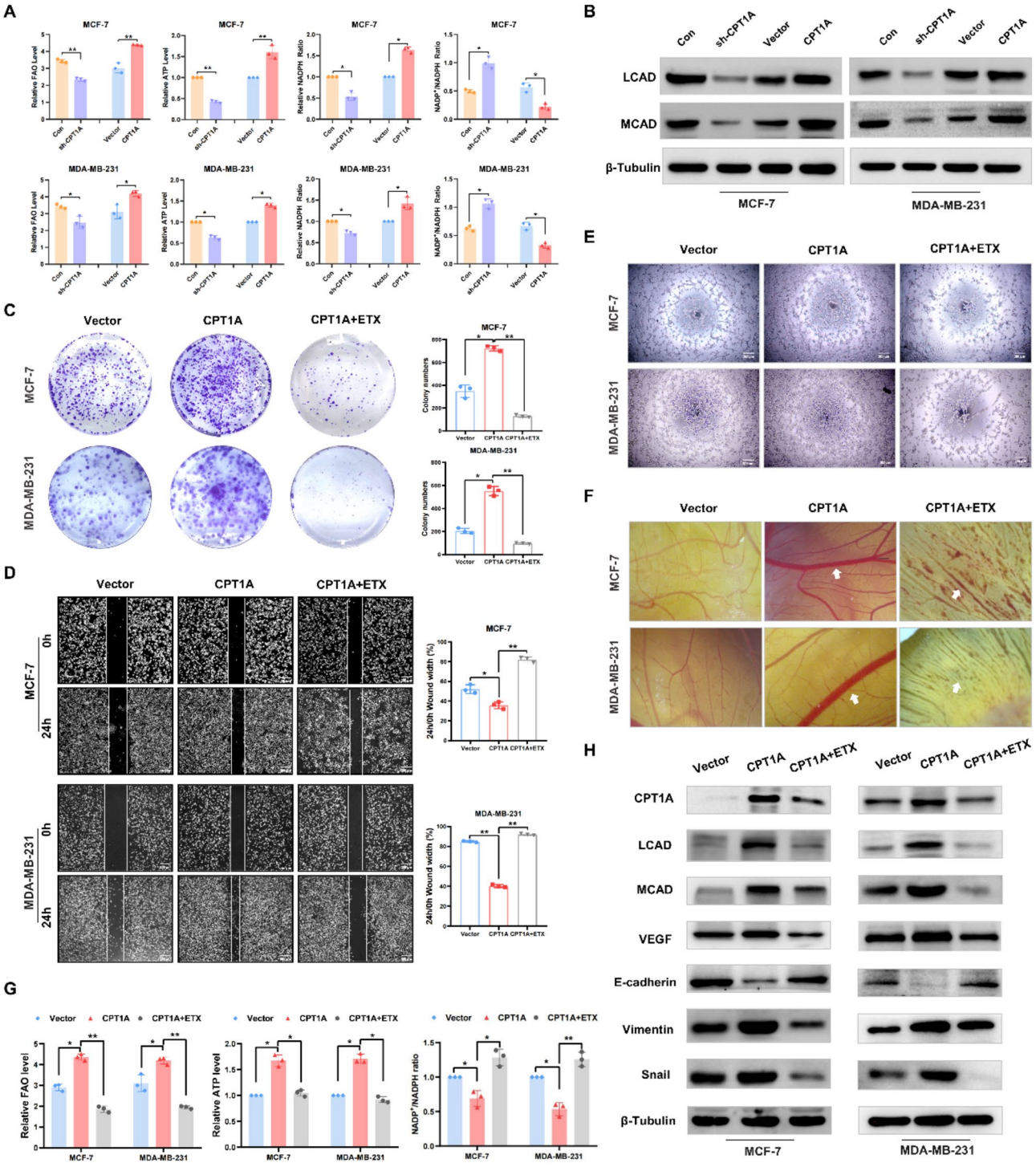

Fig. 5 CPT1A-driven FAO pathway promotes BC progression. (**A**) The production levels of FAO, ATP and NADPH were detected by kit assays in four groups of BC cells. Data were presented as the mean ± SD. (**B**) Protein expression of FAO markers (LCAD, MCAD) was detected by Western blot in CPT1A differentially expressed BC cells. (**C-D**) Colony formation (**C**) and wound healing (**D**) assays were used to test the proliferation and migration abilities of CPT1A overexpression cell after adding ETX. (**E-F**) The vascular mimicry ability of the CPT1A overexpression cell after adding ETX was detected by the microtubule formations assay (**E**). The effect of CPT1A on ex vivo angiogenesis was assessed by CAM assay. The white arrows indicate the morphological changes in CAM (**F**). (**G**) Metabolic kits were detected the FAO, ATP, and NADPH levels in CPT1A overexpression cell after adding ETX. (**H**) Protein expression of FAO, angiogenesis and EMT markers was detected by Western blot in CPT1A overexpression cell after adding ETX. $^{*}P < 0.05$, $^{**}P < 0.01$

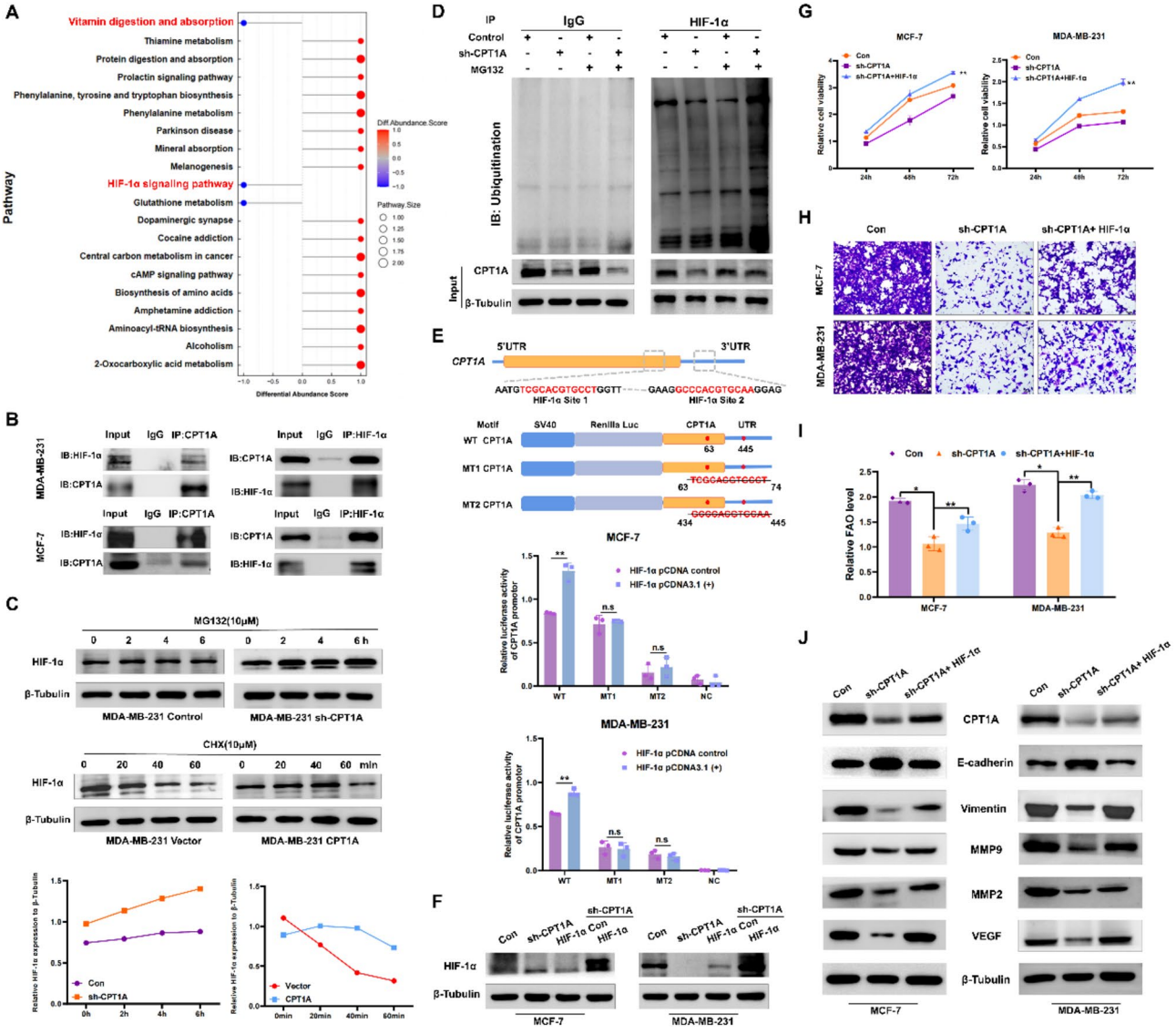

Fig. 6 The CPT1A/HIF-1α positive feedback loop promotes the proliferation and metastasis of BC. (**A**) KEGG pathway analyzed the signaling pathways of extracellular differential expression in CPT1A knockdown MDA-MB-231 cells. (**B**) The interaction between endogenous CPT1A and HIF-1α protein was analyzed by Co-IP assay. (**C**) MDA-MB-231 cells of vector and CPT1A overexpression groups were treated with 10 μM CHX for 0, 20, 40, and 60 min, then cells were collected and lysed respectively. The half-life of HIF-1α protein was detected by Western blotting and quantified by Prism Software. MDA-MB-231 cells of Control and sh-CPT1A groups were treated with 10 μM MG132 for 0, 2, 4, and 6 h, and the expression level of HIF-1α by Western blot and quantitatively analyzed. (**D**) MDA-MB-231 cells of control and sh-CPT1A groups were pretreated with 10 μM MG132 for 8 h. The ubiquitination levels of HIF-1α were measured by IP experiments. Meanwhile, the expression of CPT1A in the input samples was detected. (**E**) The binding site of HIF-1α and CPT1A promoter was predicted by the JASPAR website (UP). WT and MT1, MT2 luciferase reporter gene vectors in CPT1A 3′-UTR were co-transfected with HIF-1α control or overexpressed plasmid for 48 h in BC cells, and the luciferase activities were measured by dual-luciferase assay. Relative luciferase activity was computed by the ratio of Firefly and Renilla luciferase values. (**F**) The expression level of HIF-1α was detected by Western blot for confirming the transfected effects of HIF-1α overexpression in BC cells. (**G-H**) The proliferation ability of BC cells in the Con group, sh-CPT1A group, and sh-CPT1A + HIF-1α overexpression group was evaluated using the CCK8 assay (**G**) and the transwell migration assay (**H**). (**I**) The level of FAO in the supernatant of the three groups of cells was detected by FAO kit assay. (**J**) The levels of EMT and angiogenesis markers were detected in the three groups using Western blot. $^{*}P < 0.05$ and $^{**}P < 0.01$, N.S was represented for no statistical significance

and aggressive ovarian cancer cells, respectively [37, 38]. Furthermore, estrogen mediates hepatoprotective effects through a CPT1A-dependent FAO mechanism and inhibits prostate cancer growth by regulating ROS levels via CPT1A [39]. Our findings also demonstrated that CPT1A overexpression correlates with poorer BC patient prognosis and stimulates angiogenesis and proliferation by maintaining redox homeostasis through NADPH production. The diverse mechanisms by which CPT1A promotes tumor cell survival suggest that targeting CPT1A

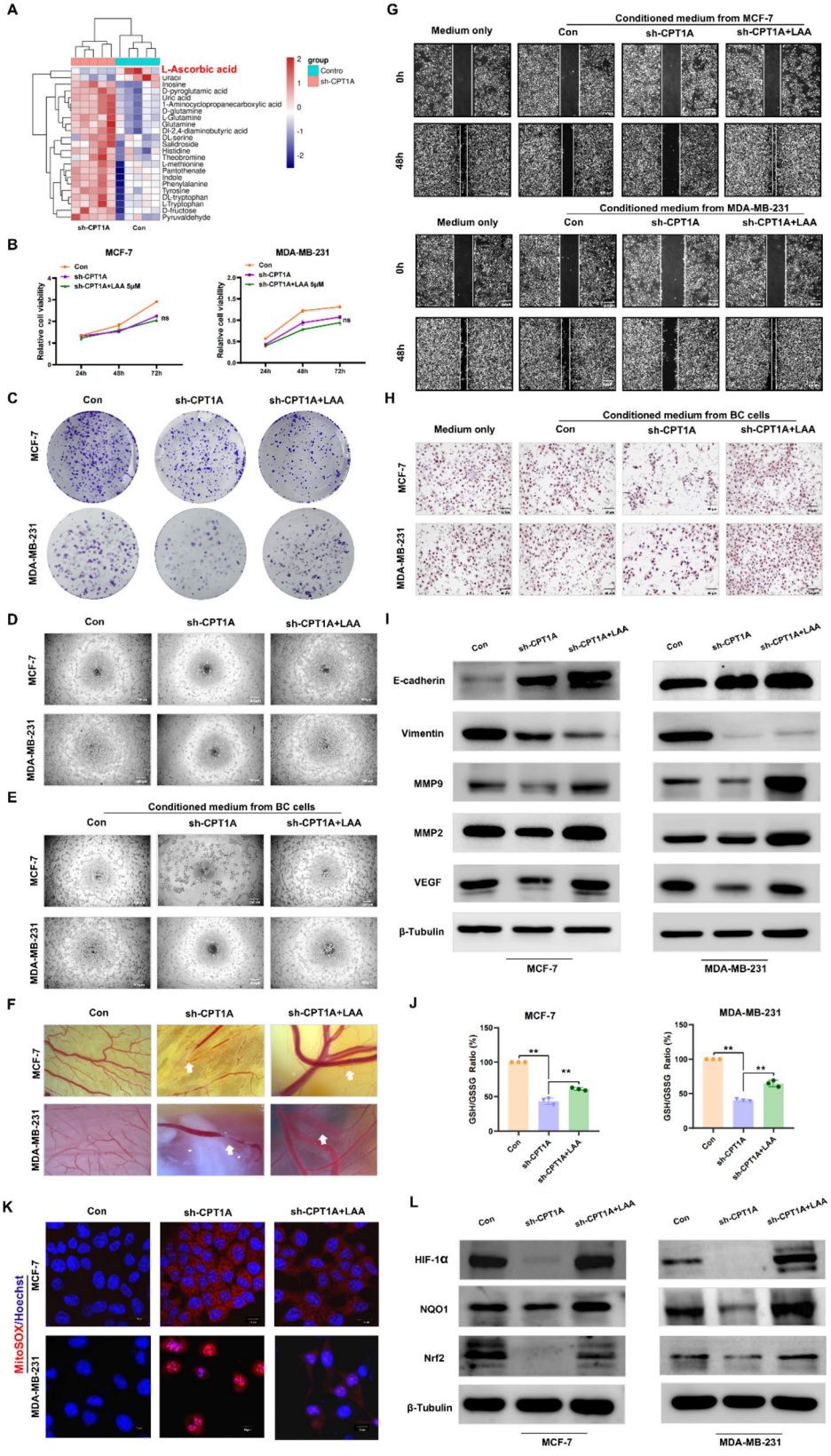

Fig. 7 (See legend on next page.)

(See figure on previous page.)

Fig. 7 LAA uptake reduced by CPT1A/HIF-1α only promotes the angiogenesis via Nrf2/NQO1 pathway. (**A**) LC-MS/MS analysis of differential metabolites in the extracellular supernatant of MDA-MB-231 cells following CPT1A knockdown. (**B-C**) CCK8 (**B**) and colony formation (**C**) assays were used to evaluate the proliferation of CPT1A knockdown cells after the addition of LAA (5 μM) in the sh-CPT1A group. (**D**) Matrigel tube formation assay detected the HUVECs tube formation ability after adding LAA (5 μM) in sh-CPT1A group. (**E**) The vascular mimicry ability of the BC cells after adding LAA (5 μM) in sh-CPT1A group was detected by the vasculogenic mimicry assay. (**F**) The effect of CPT1A knockdown cells after adding LAA (5 μM) on ex vivo angiogenesis was assessed by CAM assay. The white arrows indicate the morphological changes in CAM. (**G-H**) HUVECs were cultured with medium and the supernatants of BC cells and LAA (5 μM) respectively. The migration ability of HUVECs was assessed by wound healing (**G**) and transwell assays (**H**). (**I**) Western blot was measured the expression levels of EMT and angiogenesis markers. (**J**) The level of GSH/GSSG in the supernatant of the three groups of cells was detected by GSH/GSSG kit assay. (**K**) Representative IF staining images showing ROS expression in sh-CPT1A after adding LAA (5 μM). Scale bar: 15 μm. (**L**) Protein expression of HIF-1α, Nrf2 and NQO1 were detected by Western blot in sh-CPT1A after adding LAA (5 μM). $^{*}P < 0.05$ and $^{**}P < 0.01$. ns was represented for no statistical significance

to reduce proliferation and angiogenesis in BC cells could be an effective therapeutic strategy. Thus, we hypothesized that although CPT1A-driven FAO regulates angiogenesis and metastasis in BC cells, it is more likely to play a supporting role by altering metabolite alterations in mitochondria.

The transcription factor HIF-1α is essential in tumorigenesis, metabolism, immune evasion, and angiogenesis in BC [40, 41]. HIF-1α facilitates the conversion of glucose to pyruvate and lactate, thereby increasing ATP production and promoting BC cell proliferation [42, 43]. A reciprocal feedback loop involving HIF-1α and HPIP enhances cell migration, invasion, EMT, and metastatic characteristics in BC cells [44]. Moreover, multiple studies have demonstrated that HIF-1α facilitates the progression of papillary thyroid cancer and prostate cancer by enhancing the CPT1A-driven FAO pathway [45, 46]. Li et al. demonstrated that HIF-1α activates CPT1A, leading to increased FAO products and accelerated healing of ischemic intestinal injury [47]. Importantly, our results suggest that the CPT1A/HIF-1α positive feedback loop promotes BC proliferation and angiogenesis. Similarly, Zhang et al. demonstrated that GDF11 promotes endothelial progenitor cell mobilization and neovascularization through the HIF-1α-VEGF/SDF-1α pathway [48].

And in recent years, extracellular metabolites and nutrients have been recognized as key factors promoting tumor growth [49, 50]. Increasing evidence suggests that combining dietary therapy, nutrient deprivation, and lipid metabolism targeting represents a promising strategy for overcoming BC [51–55]. Previous studies have shown that upregulating CPT1A enhances FAO metabolism and M2 polarization of tumor-associated macrophages (TAMs), thereby promoting colorectal cancer progression [55]. One potential mechanism underlying the carcinogenic role of CPT1A in prostate cancer involves regulating the production of toxic metabolites such as ceramides and their precursors (oleyl- and palmitoyl-CoA) [56]. Interestingly, CPT1A knockdown decreases the deoxynucleotide triphosphate (dNTP) pool, disrupting HUVEC sprouting in vitro. Additionally, silencing CPT1A reduces lymphangiogenesis in BC cells by impairing VEGFR-3 expression in HDLEC cells, which can be reversed by acetate supplementation [29]. Our findings confirmed that CPT1A-driven FAO metabolism increases HUVECs proliferation and migration by elevating ATP and NADPH levels. This suggests that CPT1A may promote cancer angiogenesis in lymphatic endothelial cells and/or HUVECs via metabolic intermediates. Importantly, we demonstrated that CPT1A knockdown markedly reduces LAA levels in the supernatant, and the antioxidant effects of LAA depend on HIF-1α activation. Previous studies indicate that LAA deficiency affects the deposition of mature collagen in blood vessels [57, 58], impairing vascular formation and reducing angiogenesis [59, 60]. Furthermore, LAA regulates HIF-1α expression by reducing Fe^{3+} to Fe^{2+} and promoting α-ketoglutarate production [61]. Wang et al. reported that exposure to antioxidants for 7 days increases HIF-1α expression in tumor cells, which subsequently promotes tumor angiogenesis and VEGF production [62, 63]. This may be related to the role of ascorbic acid in hydroxylating HIF-1α, thereby regulating processes such as angiogenesis. Over recent years, ROS production has been recognized as profoundly influencing inflammatory responses and tumor progression. ROS activates various transcription factors, including HIF-1α and STAT3, creating a complex link between ROS expression and tumor progression [64]. In this study, we confirmed that LAA promotes BC angiogenesis by maintaining ROS homeostasis through enhanced HIF-1α expression or activation of the oxidative stress pathway (Nrf2/NQO1). Thus, we hypothesize that the CPT1A/HIF-1α axis could serve as a promising target for antivascular therapy in BC.

Similarly, VEGF, a critical marker of angiogenesis, was observed to be highly expressed in BC tissues and correlated with unfavorable prognosis. We propose that the CPT1A/VEGF axis may serve as a reliable prognostic marker for BC. Nonetheless, our study is not without limitations. First, the sample size was relatively small, preventing the inclusion of a more comprehensive dataset of patient cases. Second, the metabolic changes of LAA in vivo were not thoroughly investigated.

In conclusion, CPT1A drives the proliferation, metastasis, and angiogenesis of BC by activating the FAO metabolic pathway. Notably, CPT1A and HIF-1α form a

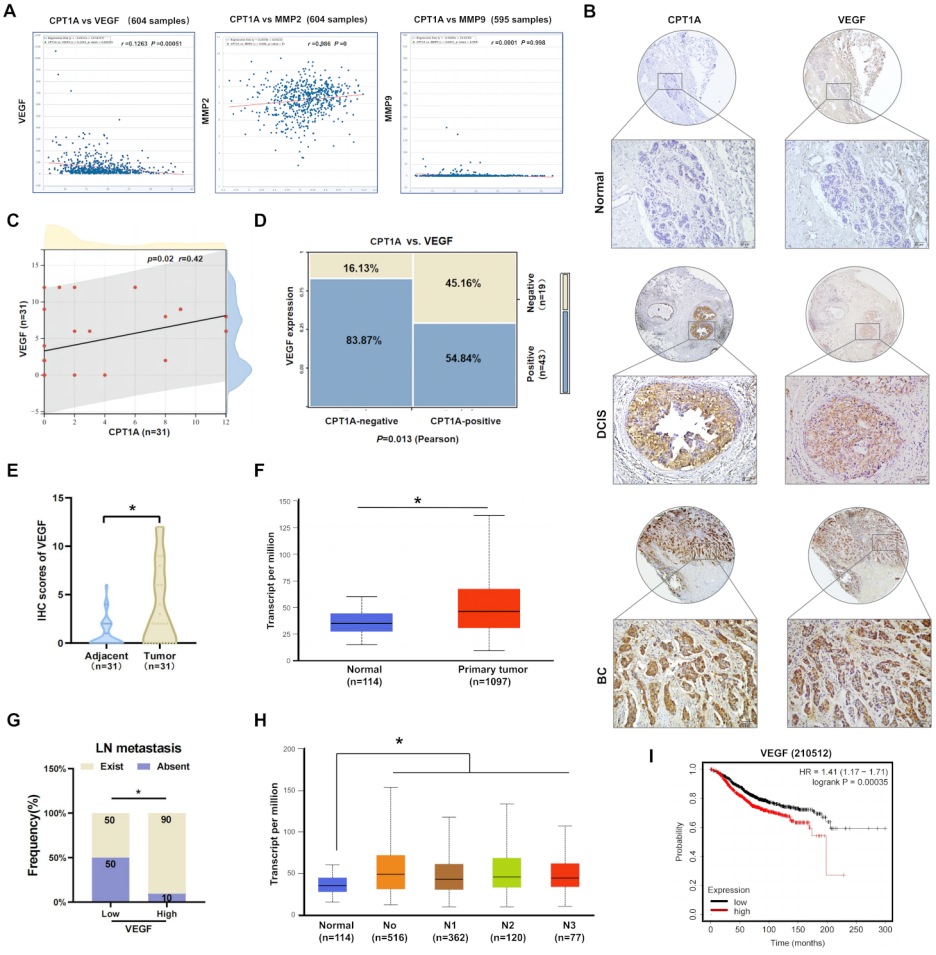

Fig. 8 High levels of CPT1A/VEGF expression are correlated with poor prognosis of patients with BC. (**A**) Chipbase database was used to search the correlation of CPT1A with VEGF, MMP2 and MMP9 in blood vessels. (**B**) Representative IHC staining images showing CPT1A and VEGF expression in normal tissues, DCIS, and BC ($n = 31$). Scale bar: 200 μm (Up), 50 μm (Down). (**C**) Correlation between CPT1A expression and VEGF expression based on the IHC scores. (**D**) JMP software was used for statistics and cartogram. (**E**) Expression level of VEGF in BC and adjacent tissues. (**F**) The expression level of VEGF in BC tissues was found by Ualcan database. (**G**) Distribution of existing and absent LN metastasis in the VEGF-low and VEGF-high groups. Chi-square test was used to test VEGF and clinicopathological parameters of BC. (**H**) Ualcan database was used to search the relationship between VEGF and LN metastasis in BC tissues. (**I**) Overall survival of BC patients with low or high VEGF expression in the Kaplan-Meier database. $^{*}P < 0.05$ and $^{**}P < 0.01$

reciprocal feedback loop: CPT1A regulates the ubiquitination and protein stability of HIF-1α, while HIF-1α, in turn, governs the transcriptional regulation of CPT1A. This CPT1A/HIF-1α positive feedback loop plays a critical role in enhancing angiogenesis in BC cells and HUVECs by modulating LAA uptake. Mechanistically, this process activates the Nrf2/NQO1 pathway to maintain ROS homeostasis. Furthermore, elevated expression levels of CPT1A and VEGF are strongly linked to poor prognosis in BC patients. These findings highlight the potential of targeting metabolic reprogramming and incorporating nutritional therapy as a novel and promising approach for BC treatment.

Abbreviations

ATCC	American Type Tissue Cultures
BC	Breast cancer
CPT1A	Carnitine palmitoyltransferase-1 A
CAM	Chorioallantoic membrane
DCIS	Ductal carcinoma in situ
DMEM	Dulbecco's Modified Eagle Medium
EMT	Epithelial-mesenchymal transition
ETX	Etomoxir
FBS	Fetal bovine serum
FAO	Fatty acid oxidation
HUVECs	Human umbilical vein endothelial cells
HIF-1α	Hypoxia-inducible factor 1-alpha
HR	Hazard ratios
LAA	L-Ascorbic acid
LN	Lymph node
LC-MS	Liquid chromatography-mass spectrometry
MMP2	Matrix metalloproteinase 2
MMP9	Matrix metalloproteinase 9
VEGF	Vascular endothelial growth factor
WHO	World Health Organization
ROS	Reactive oxygen species
TAMs	Tumor-associated macrophages

Supplementary Information

The online version contains supplementary material available at https://doi.org/10.1186/s13058-025-02039-0.

Supplementary Material 1

Supplementary Material 2

Supplementary Material 3

Supplementary Material 4

Supplementary Material 5

Supplementary Material 6

Supplementary Material 7

Supplementary Material 8

Supplementary Material 9

Supplementary Material 10

Acknowledgements
Not applicable.

Author contributions
Z-XC and YY were involved in conception and design of the study, MX and Z-BJ performed in vitro experiments and drafting of the manuscript; Y-XZ and Y-SP performed in vivo experiments and data analysis; MX, Z-BJ, and Y-XZ were involved in performing experiments and statistical analysis; L-ZH, Z-XC, and YY were manuscript revisions. All authors listed approved the final version of the manuscript.

Funding
This research was supported by the National Natural Science Foundation of China (No.82160552), and the Projects of Science and Technology Department of Jilin Province (YDZJ202201ZYTS245, YDZJ202301ZYTS127,).

Data availability
No datasets were generated or analysed during the current study.

Declarations

Ethics approval and consent to participate
The animal experiments were conducted in accordance with the regulations of the Institutional Animal Care and Use Committee with the approval of the Ethics Committee of Yanbian University.

Consent for publication
Not applicable.

Competing interests
The authors declare no competing interests.

Author details
[1]Central Laboratory, Yanbian University Hospital, Yanji 133000, PR China
[2]Key Laboratory of Tumor Pathobiology, Yanbian University, State Ethnic Affairs Commission, Yanji 133000, PR China

Received: 29 January 2025 / Accepted: 30 April 2025
Published online: 12 May 2025

References

1. Dawson S-J, Tsui DWY, Murtaza M, Biggs H, Rueda OM, Chin S-F, Dunning MJ, Gale D, Forshew T, Mahler-Araujo B, et al. Analysis of Circulating tumor DNA to monitor metastatic breast cancer. N Engl J Med. 2013;368(13):1199–209.
2. Schneider BP, Miller KD. Angiogenesis of breast cancer. J Clin Oncol. 2005;23(8):1782–90.
3. Caswell-Jin JL, Sun LP, Munoz D, Lu Y, Li Y, Huang H, Hampton JM, Song J, Jayasekera J, Schechter C, et al. Analysis of breast Cancer mortality in the US-1975 to 2019. JAMA. 2024;331(3):233–41.
4. Zeng H, Hou Y, Zhou X, Lang L, Luo H, Sun Y, Wan X, Yuan T, Wang R, Liu Y, et al. Cancer-associated fibroblasts facilitate premetastatic niche formation through LncRNA SNHG5-mediated angiogenesis and vascular permeability in breast cancer. Theranostics. 2022;12(17):7351–70.
5. Cao Y, Arbiser J, D'Amato RJ, et al. Forty-year journey of angiogenesis translational research. Sci Transl Med. 2011;3(114):114rv3.
6. Van Cutsem E, Vervenne WL, Bennouna J, et al. Phase III trial of bevacizumab in combination with gemcitabine and erlotinib in patients with metastatic pancreatic cancer. J Clin Oncol. 2009;27(13):2231–7.
7. Beloribi-Djefaflia S, Vasseur S, Guillaumond F. Lipid metabolic reprogramming in cancer cells. Oncogenesis. 2016;5(1):e189. Published 2016 Jan 25.
8. Caro P, Kishan AU, Norberg E, et al. Metabolic signatures uncover distinct targets in molecular subsets of diffuse large B cell lymphoma. Cancer Cell. 2012;22(4):547–60.
9. Liu Y, Zuckier LS, Ghesani NV. Dominant uptake of fatty acid over glucose by prostate cells: a potential new diagnostic and therapeutic approach. Anticancer Res. 2010;30(2):369–74.
10. Puca F, Yu F, Bartolacci C, et al. Medium-Chain Acyl-CoA dehydrogenase protects mitochondria from lipid peroxidation in glioblastoma. Cancer Discov. 2021;11(11):2904–23.
11. Ranea-Robles P, Pavlova NN, Bender A, et al. A mitochondrial long-chain fatty acid oxidation defect leads to transfer RNA uncharging and activation of the integrated stress response in the mouse heart. Cardiovasc Res. 2022;118(16):3198–210.
12. Reilly PT, Mak TW. Molecular pathways: tumor cells Co-opt the brain-specific metabolism gene CPT1C to promote survival. Clin Cancer Res. 2012;18(21):5850–5.
13. Li X, Kumar A, Carmeliet P. Metabolic pathways fueling the endothelial cell drive. Annu Rev Physiol. 2019;81:483–503.
14. Li R, Li X, Zhao J, Meng F, Yao C, Bao E, Sun N, Chen X, Cheng W, Hua H, et al. Mitochondrial STAT3 exacerbates LPS-induced sepsis by driving CPT1a-mediated fatty acid oxidation. Theranostics. 2022;12(2):976–98.
15. He Q, Yang J, Pan Z, Zhang G, Chen B, Li S, Xiao J, Tan F, Wang Z, Chen P, et al. Biochanin A protects against iron overload associated knee osteoarthritis via regulating iron levels and NRF2/System xc-/GPX4 axis. Biomed Pharmacother. 2023;157:113915.
16. Bensaad K, Favaro E, Lewis CA, et al. Fatty acid uptake and lipid storage induced by HIF-1α contribute to cell growth and survival after hypoxia-reoxygenation. Cell Rep. 2014;9(1):349–65.
17. Casanovas O, Hicklin DJ, Bergers G, Hanahan D. Drug resistance by evasion of antiangiogenic targeting of VEGF signaling in late-stage pancreatic islet tumors. Cancer Cell. 2005;8(4):299–309.
18. Cao Y, Zhong W, Sun Y. Improvement of antiangiogenic cancer therapy by Understanding the mechanisms of angiogenic factor interplay and drug resistance. Semin Cancer Biol. 2009;19(5):338–43.
19. Hecht F, Zocchi M, Alimohammadi F, Harris IS. Regulation of antioxidants in cancer. Mol Cell. 2024;84(1):23–33.
20. Qin L-N, Zhang H, Li Q-Q, Wu T, Cheng S-B, Wang K-W, Shi Y, Ren H-R, Xing X-W, Yang C, et al. Vitamin D binding protein (VDBP) hijacks twist1 to inhibit vasculogenic mimicry in hepatocellular carcinoma. Theranostics. 2024;14(1):436–50.
21. Lykkesfeldt J, Carr AC. Vitamin C. Adv Nutr. 2024;15(1):100155.
22. Tyuryaeva I, Lyublinskaya O. Expected and unexpected effects of Pharmacological antioxidants. Int J Mol Sci 2023, 24(11).
23. Yun J, Mullarky E, Lu C, et al. Vitamin C selectively kills KRAS and BRAF mutant colorectal cancer cells by targeting GAPDH. Science. 2015;350(6266):1391–6.
24. Schoenfeld JD, Sibenaller ZA, Mapuskar KA, et al. O2·- and H2O2-Mediated disruption of Fe metabolism causes the differential susceptibility of NSCLC and GBM Cancer cells to Pharmacological ascorbate. Cancer Cell. 2017;32(2):268.
25. Cameron E, Pauling L. Supplemental ascorbate in the supportive treatment of cancer: Reevaluation of prolongation of survival times in terminal human cancer. Proc Natl Acad Sci U S A. 1978;75(9):4538–42.
26. Cameron E, Campbell A. The orthomolecular treatment of cancer. II. Clinical trial of high-dose ascorbic acid supplements in advanced human cancer. Chem Biol Interact. 1974;9(4):285–315.
27. Yan H, Malik N, Kim Y-I, He Y, Li M, Dubois W, Liu H, Peat TJ, Nguyen JT, Tseng Y-C, et al. Fatty acid oxidation is required for embryonic stem cell survival during metabolic stress. EMBO Rep. 2021;22(6):e52122.

28. Wang X, Liu Y, Han A, et al. The NQO1/p53/SREBP1 axis promotes hepatocellular carcinoma progression and metastasis by regulating snail stability. Oncogene. 2022;41(47):5107–20.
29. Xiong Y, Liu Z, Zhao X, Ruan S, Zhang X, Wang S, Huang T. CPT1A regulates breast cancer-associated lymphangiogenesis via VEGF signaling. Biomed Pharmacother. 2018;106:1–7.
30. Griffioen AW, Dudley AC. The rising impact of angiogenesis research. Angiogenesis. 2022;25(4):435–7.
31. Schlüter A, Weller P, Kanaan O, Nel I, Heusgen L, Höing B, Haßkamp P, Zander S, Mandapathil M, Dominas N, et al. CD31 and VEGF are prognostic biomarkers in early-stage, but not in late-stage, laryngeal squamous cell carcinoma. BMC Cancer. 2018;18(1):272.
32. Wan X, Guan S, Hou Y, Qin Y, Zeng H, Yang L, Qiao Y, Liu S, Li Q, Jin T, et al. FOSL2 promotes VEGF-independent angiogenesis by transcriptionnally activating Wnt5a in breast cancer-associated fibroblasts. Theranostics. 2021;11(10):4975–91.
33. Al Kawas H, Saaid I, Jank P, Westhoff CC, Denkert C, Pross T, Weiler KBS, Karsten MM. How VEGF-A and its splice variants affect breast cancer development - clinical implications. Cell Oncol (Dordr). 2022;45(2):227–39.
34. Ma L, Chen C, Zhao C, Li T, Ma L, Jiang J, Duan Z, Si Q, Chuang T-H, Xiang R, et al. Targeting carnitine palmitoyl transferase 1A (CPT1A) induces ferroptosis and synergizes with immunotherapy in lung cancer. Signal Transduct Target Ther. 2024;9(1):64.
35. Weiss F, Lauffenburger D, Friedl P. Towards targeting of shared mechanisms of cancer metastasis and therapy resistance. Nat Rev Cancer. 2022;22(3):157–73.
36. Tang M, Dong X, Xiao L, Tan Z, Luo X, Yang L, Li W, Shi F, Li Y, Zhao L, et al. CPT1A-mediated fatty acid oxidation promotes cell proliferation via nucleoside metabolism in nasopharyngeal carcinoma. Cell Death Dis. 2022;13(4):331.
37. Wang Y-N, Zeng Z-L, Lu J, Wang Y, Liu Z-X, He M-M, Zhao Q, Wang Z-X, Li T, Lu Y-X, et al. CPT1A-mediated fatty acid oxidation promotes colorectal cancer cell metastasis by inhibiting Anoikis. Oncogene. 2018;37(46):6025–40.
38. Sawyer BT, Qamar L, Yamamoto TM, McMellen A, Watson ZL, Richer JK, Behbakht K, Schlaepfer IR, Bitler BG. Targeting fatty acid oxidation to promote Anoikis and inhibit ovarian Cancer progression. Mol Cancer Res. 2020;18(7):1088–98.
39. Jiang C, Zhu Y, Chen H, Lin J, Xie R, Li W, Xue J, Chen L, Chen X, Xu S. Targeting c-Jun inhibits fatty acid oxidation to overcome Tamoxifen resistance in Estrogen receptor-positive breast cancer. Cell Death Dis. 2023;14(10):653.
40. Schmid T, Zhou J, Brüne B. HIF-1 and p53: communication of transcription factors under hypoxia. J Cell Mol Med. 2004;8(4):423–31.
41. Lei J, Jiang X, Huang D, Jing Y, Yang S, Geng L, Yan Y, Zheng F, Cheng F, Zhang W, et al. Human ESC-derived vascular cells promote vascular regeneration in a HIF-1α dependent manner. Protein Cell. 2024;15(1):36–51.
42. Owczarek A, Gieczewska KB, Jarzyna R, Frydzinska Z, Winiarska K. Transcription factor ChREBP mediates high Glucose-Evoked increase in HIF-1α content in epithelial cells of renal proximal tubules. Int J Mol Sci. 2021;22(24):13299.
43. Gunton JE. Hypoxia-inducible factors and diabetes. J Clin Invest. 2020;130(10):5063–73.
44. Khumukcham SS, Penugurti V, Soni A, Uppala V, Hari K, Jolly MK, Dwivedi A, Salam Pk A, Padala C, Mukta S, et al. A reciprocal feedback loop between HIF-1α and HPIP controls phenotypic plasticity in breast cancer cells. Cancer Lett. 2022;526:12–28.
45. Liang Z, He H, Zhang B, Kai Z, Zong L. Hypoxia expedites the progression of papillary thyroid carcinoma by promoting the CPT1A-mediated fatty acid oxidative pathway. Drug Dev Res. 2024;85(2):e22168.
46. Rios-Colon L, Kumar P, Kim S, Sharma M, Su Y, Kumar A, Singh S, Stocks N, Liu L, Joshi M et al. Carnitine Palmitoyltransferase 1 Regulates Prostate Cancer Growth under Hypoxia. *Cancers (Basel)* 2021, 13(24).
47. Li L, Liu Y, Zhi N, Ji Y, Xu J, Mao G, Wang Y, Ma J, Wang Y. Hypoxic preconditioning accelerates the healing of ischemic intestinal injury by activating HIF-1α/PPARα pathway-mediated fatty acid oxidation. Cell Death Discov. 2024;10(1):164.
48. Zhang Y, Zhang Y-Y, Pan Z-W, Li Q-Q, Sun L-H, Li X, Gong M-Y, Yang X-W, Wang Y-Y, Li H-D, et al. GDF11 promotes wound healing in diabetic mice via stimulating HIF-1α-VEGF/SDF-1α-mediated endothelial progenitor cell mobilization and neovascularization. Acta Pharmacol Sin. 2023;44(5):999–1013.
49. Zhang Y, Liang F, Zhang D, Qi S, Liu Y. Metabolites as extracellular vesicle cargo in health, cancer, pleural effusion, and cardiovascular diseases: an emerging field of study to diagnostic and therapeutic purposes. Biomed Pharmacother. 2023;157:114046.
50. Pathan M, Fonseka P, Chitti SV, Kang T, Sanwlani R, Van Deun J, Hendrix A, Mathivanan S. Vesiclepedia 2019: a compendium of RNA, proteins, lipids and metabolites in extracellular vesicles. Nucleic Acids Res. 2019;47(D1):D516–9.
51. Steidl ME, Nigro EA, Nielsen AK, Pagliarini R, Cassina L, Lampis M, Podrini C, Chiaravalli M, Mannella V, Distefano G, et al. Primary cilia sense glutamine availability and respond via asparagine synthetase. Nat Metab. 2023;5(3):385–97.
52. Gameiro PA, Struhl K. Nutrient deprivation elicits a transcriptional and translational inflammatory response coupled to decreased protein synthesis. Cell Rep. 2018;24(6):1415–24.
53. Haferkamp S, Drexler K, Federlin M, Schlitt HJ, Berneburg M, Adamski J, Gaumann A, Geissler EK, Ganapathy V, Parkinson EK, et al. Extracellular citrate fuels Cancer cell metabolism and growth. Front Cell Dev Biol. 2020;8:602476.
54. Zhong J, Li P, Zheng F, Li Y, Lu W, Chen H, Cai J, Xia D, Wu Y. Association between dietary vitamin C intake/blood level and risk of digestive system cancer: a systematic review and meta-analysis of prospective studies. Food Funct. 2024;15(16):8217–37.
55. Sun M, Yue Y, Wang X, Feng H, Qin Y, Chen M, Wang Y, Yan S. ALKBH5-mediated upregulation of CPT1A promotes macrophage fatty acid metabolism and M2 macrophage polarization, facilitating malignant progression of colorectal cancer. Exp Cell Res. 2024;437(1):113994.
56. Guth A, Monk E, Agarwal R, Bergman BC, Zemski-Berry KA, Minic A, Jordan K, Schlaepfer IR. Targeting fat oxidation in mouse prostate Cancer decreases tumor growth and stimulates Anti-Cancer immunity. Int J Mol Sci. 2020;21(24):9660.
57. De Tullio MC, Arrigoni O. Hopes, disillusions and more hopes from vitamin C. Cell Mol Life Sci. 2004;61(2):209–19.
58. Murad S, Grove D, Lindberg KA, Reynolds G, Sivarajah A, Pinnell SR. Regulation of collagen synthesis by ascorbic acid. Proc Natl Acad Sci U S A. 1981;78(5):2879–82.
59. Jalil ZH, Sahib HB. Antiangiogenic activity of quinine alone and in combination with vitamin C in both ex vivo and in vivo assays. Asian Pac J Cancer Prev. 2022;23(12):4185–92.
60. Wenzel U, Nickel A, Kuntz S, Daniel H. Ascorbic acid suppresses drug-induced apoptosis in human colon cancer cells by scavenging mitochondrial superoxide anions. Carcinogenesis. 2004;25(5):703–12.
61. Martínez-Reyes I, Chandel NS. Mitochondrial TCA cycle metabolites control physiology and disease. Nat Commun. 2020;11(1):102.
62. Wang T, Dong Y, Huang Z, Zhang G, Zhao Y, Yao H, Hu J, Tüksammel E, Cai H, Liang N, et al. Antioxidants stimulate BACH1-dependent tumor angiogenesis. J Clin Invest. 2023;133(20):e169671.
63. Han YJ, Liu S, Hardeman A, Rajagopal PS, Mueller J, Khramtsova G, Sanni A, Ajani MA, Clayton W, Hurley IW, et al. The VEGF-Hypoxia signature is upregulated in basal like breast tumors from women of African ancestry and associated with poor outcomes in breast Cancer. Clin Cancer Res. 2024;30(11):2609–18.
64. Gupta SC, Hevia D, Patchva S, Park B, Koh W, Aggarwal BB. Upsides and downsides of reactive oxygen species for cancer: the roles of reactive oxygen species in tumorigenesis, prevention, and therapy. Antioxid Redox Signal. 2012;16(11):1295–322.

Publisher's note